AIAA JOURNAL
Vol. 39, No. 2, February 2001

Refined Structural Dynamics Model for Composite Rotor Blades

Sung Nam Jung,* V. T. Nagaraj,† and Inderjit Chopra‡
University of Maryland, College Park, Maryland 20742

A refined one-dimensional beam formulation based on a mixed approach has been developed for structural dynamics analyses of rotating and nonrotating composite beams and blades of general section shape with open- or closed-section contours. The theory uses a mixed variational approach and accounts for the effects of elastic coupling, shell-wall thickness, warping, warping restraint, and transverse shear deformations. The analysis is validated against experimental data and other analytical results for composite cantilevered beams of various cross sections. Good correlation is achieved for all of the cases considered. The influence of wall thickness and transverse shear on the free vibration characteristics of composite beams with either bending–torsion or extension–torsion coupling is investigated. For a bending–torsion coupled beam, the influence of wall thickness becomes important when the thickness-to-depth ratio of the beam reaches about 30%. The frequency error in neglecting transverse shear flexibility is about 50% for a bending–torsion coupled composite box beam with a slenderness ratio of 5.

Nomenclature

$A'_{ij}, B'_{ij}, D'_{ij}, A_{xn}$	=	modified laminate stiffnesses; Eq. (6)
$A_{n\varepsilon}, A_{n\kappa}, \ldots, A_{\gamma\tau}$	=	semi-inverted coefficients; Eq. (7a)
E_1, E_2	=	Young's moduli in principal directions
$f_x, f_y, f_z, f_\phi, f_\omega$	=	shear flow components
G_{12}	=	shear modulus
k_A^2	=	radius of gyration
M_{xx}, M_{ss}, M_{xs}	=	moments for the shell segment
M_y, M_z	=	beam bending moments
M_ω	=	warping torsion
$m_{k_{m_1}^2}, m_{k_{m_2}^2}$	=	mass moment of inertia
mk_m^2	=	polar mass moment of inertia, $mk_{m_1}^2 + mk_{m_2}^2$
N	=	axial force of beam
N_{xn}, N_{sn}	=	transverse shear stress resultants for the shell
N_{xx}, N_{ss}, N_{xs}	=	membrane stress resultants for the shell segment
Q_y, Q_z	=	transverse shear forces
T_s	=	St. Venant torque
U, V, W	=	beam displacements
u, v_t, v_n	=	shell-wall displacements; Eq. (1)
x, s, n	=	coordinate systems of shell wall
x, y, z	=	undeformed beam coordinates
β_y, β_z	=	cross section rotations of beam
γ_{xn}	=	transverse shear strain of shell
γ_{xy}, γ_{xz}	=	transverse shear strains of beam
$\varepsilon_{xx}, \varepsilon_{ss}, \varepsilon_{xs}$	=	membrane strains of shell
$\kappa_{xx}, \kappa_{ss}, \kappa_{xs}$	=	curvatures of the midsurface of shell
ν_{12}	=	Poisson's ratio in principal plane
ρ	=	mass density
Φ_R	=	semicomplementary energy function; Eq. (8)
ϕ	=	elastic twist deformation
Ω	=	rotational speed, rpm
$\bar{\omega}$	=	sectorial area; Eq. (4a)

Subscripts

$,n$	=	$\partial(\,)/\partial n$
$,s$	=	$\partial(\,)/\partial s$
$,x$	=	$\partial(\,)/\partial x$

Presented as Paper 99-1485 at the AIAA 40th Structures, Structural Dynamics, and Materials Conference, St. Louis, MO, 12–15 April 1999; received 27 August 1999; revision received 13 July 2000; accepted for publication 25 July 2000. Copyright © 2000 by the authors. Published by the American Institute of Aeronautics and Astronautics, Inc., with permission.

*Visiting Associate Professor, Alfred Gessow Rotorcraft Center, Department of Aerospace Engineering; also Associate Professor, School of Mechanical and Aerospace Engineering, Chonbuk National University, Chonju 561-756, Republic of Korea. Member AIAA.

†Research Scientist, Alfred Gessow Rotorcraft Center, Department of Aerospace Engineering.

‡Alfred Gessow Professor and Director, Alfred Gessow Rotorcraft Center, Department of Aerospace Engineering. Fellow AIAA.

I. Introduction

A CONSIDERABLE number of studies have been carried out to develop a proper methodology to analyze composite tailored rotor blades. These range from simple analytical models to detailed finite element methods. Jung et al.[1] made an assessment of the current techniques of modeling composite rotor blades and identified, among others, the need for a comprehensive generic analysis that will be applicable to blades having open or closed cross sections and that includes such features as elastic couplings and thickness of the shell wall.

Composite rotor blades are, in general, built-up structures with different materials for skin and spar and may have honeycomb/structural foam fillers for maintaining the airfoil shape along with leading-edge erosion caps, provisions for anti-icing, and balance weights. Main rotor blades are normally of closed single- or multicelled cross sections and are thin walled, except near the root, where they may be thick walled. Because of their relatively smaller chords, tail rotor blades may need to be analyzed as thick-walled structures. An accurate analysis that takes into account all of these features is a challenging task. One approach may be to use a detailed finite element analysis, for example, VABS.[2] In spite of the variety of construction features, it is possible to model rotor blades as thin-/thick-walled beams using classical lamination theory to model the structural behavior of the skin, spars, and other load bearing areas. Such a model that incorporates both Timoshenko effects and Vlasov effects is useful especially for preliminary design studies and for optimization analyses. Common to both thin-walled and thick-walled blade analysis is the need to model properly the local behavior of the shell wall as a result of the global deformation of the blade. The wall undergoes both in-plane and out-of-plane deformations (warping) in response to the applied external loading. It is important to model these warpings consistently to obtain accurate results for the beam response.[1]

The modeling of beams and blades can be formulated through either a displacement or a force approach. The displacement formulation, also called the stiffness formulation, has been used by, among others, Rehfield,[3] Rehfield et al.,[4] Smith and Chopra,[5] and Chandra and Chopra.[6,7] The stiffness formulation is based on suitable approximations to the displacement field of the shell wall. The assumed displacement field is used to compute the strain energy, and using the energy principles yields the beam stiffness relations as well as equations of motion. The displacement modes do not satisfy the equations of equilibrium of the shell wall, and this approach leads to

an overestimation of the beam stiffnesses. Cesnick and Hodges[2] and Hodges et al.[8,9] used the variational asymptotic method to derive the asymptotically correct stiffness matrix and warping displacements for nonhomogeneous and anisotropic beam cross sections. The elements of stiffness matrix are developed using a finite element technique.

In the force formulation, also called the flexibility formulation, the assumed direct stress field in the shell wall is used to obtain the distribution of the shear stress, and the related warpings are determined from the equilibrium equations of the shell wall. The flexibility method provides a systematic method of determining the warping functions. This method has been used by Mansfield and Sobey,[10] by Libove[11] and, more recently, by Johnson et al.[12] for thin-walled composite beams with closed profiles.

Berdichevsky et al.[13] and Badir et al.[14] used the variational-asymptotic approach in which the displacement approximations are refined in an iterative manner. They have applied their method to analyze thin-walled composite beams of both closed[13] and open cross sections.[14] Murakami et al.[15] proposed a Timoshenko-type beam theory based on a mixed variational principle and the use of Reissner's semicomplementary energy function.[16] They applied the theory to the bending problem of anisotropic beam with rectangular solid cross section. The distribution of shear stresses was generated as part of the solution.

Recently, Jung et al.[17] developed a general one-dimensional beam formulation based on a mixed variational approach that takes into account the effects of transverse shear deformation, warping, warping restraint, and bending and shear of the shell wall on the static analysis of composite beams with elastic couplings. The theory is termed mixed because the direct stresses are treated as the known variables in terms of assumed displacements and the shear flow in the shell walls is treated as the unknown. The main features of the present theory are 1) the influence of the thickness of the shell wall including shear deformation (Reissner–Mindlin)[18] effects are included; 2) the wall is modeled as shell; 3) it is a combination of the displacement and the force formulation, the shear flow N_{xs} is assumed as a dependent variable, and closed-form expressions are derived to express this in terms of the geometry and material distribution of the structure; 4) a plane stress assumption is used for the constitutive relations; 5) both closed and open cross section blades are treated in this unified formulation. The result is a first-order shear deformation (Timoshenko) theory for the global beam behavior.

Chandra and Chopra[6,7] have extended the Vlasov theory for thin-walled composite blades and included first-order shear deformation effects with the shear correction factors set to unity. They used a plane strain assumption ($\varepsilon_{ss} = \kappa_{ss} = 0$). In Ref. 17, a provision was made to use either the plane strain or the plane stress assumption ($N_{ss} = M_{ss} = 0$). Examples show that the plane stress assumption leads to better correlation with experimental results. The stiffness matrix derived by Chandra and Chopra[6,7] is of the order (9×9) because they include $\gamma_{xy,x}$ and $\gamma_{xz,x}$ as independent degrees of freedom in their formulation, whereas the present approach leads to (7×7) stiffness matrix.

In the present paper, the static analysis of Ref. 17 is extended to cover structural dynamics of rotating and nonrotating composite beams. The analysis is validated against experimental test data and other analyses for composite beams of various cross sections such as a box section, a rectangular solid section, and an I section. The effects of modeling refinements on the free vibration characteristics of composite beams with elastic couplings are investigated.

II. Formulation

This section briefly describes the mixed variational formulation for the analysis of composite beams with elastic couplings. The analysis covers open- and closed-section, thin- and thick-walled section, and single- and multicell section beams. Transverse shear deformation across both the shell wall and the cross section of the beam, torsion-related warping, and warping restraint effects are included in the formulation.

It is assumed that the in-plane deformations of the shell wall are negligibly small compared with the out-of-plane deformations. This assumption is more accurate for rotor blades with thick walls or whose walls are supported by honeycomb or foam cores. To include thick-walled effects, first-order shear deformation theory is used to model the shell wall. Note that this includes membrane and bending modes of the shell wall as subsets. For each of these modes, the global structural behavior of the blade can be modeled at various levels, for example, Euler–Bernoulli, St. Venant, Timoshenko, and Vlasov. The lateral stress and moment resultants are assumed to be negligibly small ($N_{ss} = 0$ and $M_{ss} = 0$).

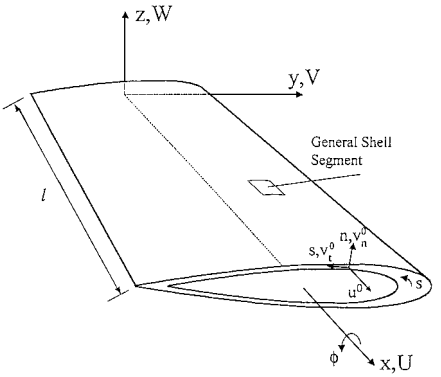

Fig. 1a Geometry and coordinate systems of a blade.

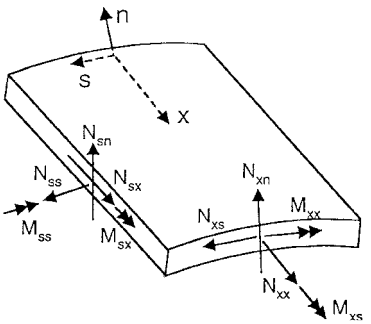

Fig. 1b Shell forces and moments.

A. Kinematics

The global deformations of the beam are U, V, and W along the x, y, and z axes, and ϕ is the twist about the x axis (Fig. 1). The local shell deformations are u, v_t, and v_n along the x, s, and n directions, respectively.

When transverse shear deformations are allowed for, the local deformations at an arbitrary point on the shell wall can be expressed as

$$u = u^0 + n\psi_x, \qquad v_t = v_t^0 + n\psi_s, \qquad v_n = v_n^0 \tag{1}$$

In Eq. (1), u^0, v_t^0, and v_n^0 represent the deformations at the midplane of the shell and ψ_x and ψ_s represent rotations of the normals to the midplane about the s and x axes, respectively. By the use of the strain-displacement and curvature-displacement relations for the wall of a cylindrical shell of arbitrary geometry, and by the assumption of negligibly small in-plane deformations, the shell midplane displacements can be obtained in terms of the beam displacements and rotations as

$$v_t^0 = Vy_{,s} + Wz_{,s} + r\phi, \qquad v_n^0 = Vz_{,s} - Wy_{,s} - q\phi$$
$$\psi_s = \phi \tag{2}$$

The shell rotation ψ_x can be obtained by equating the shear strain γ_{xn} from the beam kinematics to its value from the shell deformation:

$$\psi_x = \gamma_{xn} - v_{n,x}^0 = \gamma_{xy}z_{,s} - \gamma_{xz}y_{,s} \tag{3}$$

In Eq. (3), γ_{xy} and γ_{xz} represent the shear strain of the blade and are related to β_y and β_z (the rotations of the blade cross section about the y and z axes, respectively) as

$$\beta_y = \gamma_{xz} - W_{,x}, \qquad \beta_z = \gamma_{xy} - V_{,x} \tag{3a}$$

The axial displacement u^0 consists of 1) axial displacement of the beam, 2) axial warping due to bending, 3) axial warping due to torsion, and 4) axial warping due to transverse shear. From the expression for the shear strain, we can get[17]

$$u^0 = U + y\beta_z + z\beta_y - \bar{\omega}\phi_{,x} \tag{4}$$

where the sectorial area $\bar{\omega}$ is defined as

$$\bar{\omega} = \int_0^s r\,\mathrm{d}s \tag{4a}$$

By the use of the relation in Eq. (4), the strain-displacementrelations can be written as

$$\begin{aligned}
\varepsilon_{xx} &= U_{,x} + z\beta_{y,x} + y\beta_{z,x} - \bar{\omega}\phi_{,xx}\\
\gamma_{xs}^k &= u_{,s}^0 + V_{,x}y_{,s} + W_{,x}z_{,s} + r\phi_{,x}\\
\kappa_{xx} &= \beta_{z,x}z_{,s} - \beta_{y,x}y_{,s} + q\phi_{,xx}\\
\kappa_{xs} &= 2\phi_{,x} + (1/a)(\beta_z y_{,s} + \beta_y z_{,s} - r\phi_{,x})\\
\gamma_{xn}^k &= u_{,n}^0 + V_{,x}z_{,s} - W_{,x}y_{,s} - q\phi_{,x}
\end{aligned} \tag{5}$$

The superscript k in γ_{xs}^k and γ_{xn}^k is used to denote that these strain-displacement relations are obtained from kinematic considerations.

B. Constitutive Relations

Under the assumption that the in-plane stress and moment resultants, as well as the transverse shear stress resultant, are negligible, ε_{ss}, κ_{ss}, and γ_{sn} can be expressed in terms of the other strains. The constitutive relations for the shell wall can be expressed as

$$\begin{Bmatrix} N_{xx}\\ N_{xs}\\ M_{xx}\\ M_{xs}\end{Bmatrix} = \begin{bmatrix} A'_{11} & A'_{16} & B'_{11} & B'_{16}\\ A'_{16} & A'_{66} & B'_{16} & B'_{66}\\ B'_{11} & B'_{16} & D'_{11} & D'_{16}\\ B'_{16} & B'_{66} & D'_{16} & D'_{66}\end{bmatrix} \begin{Bmatrix} \varepsilon_{xx}\\ \gamma_{xs}^c\\ \kappa_{xx}\\ \kappa_{xs}\end{Bmatrix}, \qquad N_{xn} = A_{xn}\gamma_{xn}^c \tag{6}$$

A'_{ij}, B'_{ij}, and D'_{ij} are obtained from the A_{ij}, B_{ij}, and D_{ij} coefficients of classical lamination theory.[19] In the present method, ε_{xx}, κ_{xx}, and κ_{xs} are assumed as in the displacement formulation, and N_{xs} is treated as a dependent variable and is derived from the equilibrium equations. To do this, it is convenient to write Eq. (6) in a semi-inverted form as

$$\begin{Bmatrix} N_{xx}\\ M_{xx}\\ M_{xs}\\ \gamma_{xs}^c\end{Bmatrix} = \begin{bmatrix} A_{n\varepsilon} & A_{n\kappa} & A_{n\phi} & A_{n\tau}\\ A_{n\kappa} & A_{m\kappa} & A_{m\phi} & A_{m\tau}\\ A_{n\phi} & A_{m\phi} & A_{\phi\phi} & A_{\phi\tau}\\ -A_{n\tau} & -A_{m\tau} & -A_{\phi\tau} & A_{\gamma\tau}\end{bmatrix} \begin{Bmatrix} \varepsilon_{xx}\\ \kappa_{xx}\\ \kappa_{xs}\\ N_{xs}\end{Bmatrix}$$

$$N_{xn} = A_{xn}\gamma_{xn}^c \tag{7}$$

where the stiffness coefficients A_{ij} are given by

$$\begin{aligned}
A_{n\varepsilon} &= \left[A'_{11} - \left(A'^2_{16}/A'_{66}\right)\right], \qquad A_{n\kappa} = [B'_{11} - (A'_{16}B'_{16}/A_{66})]\\
A_{n\phi} &= [B'_{16} - (A'_{16}B'_{66}/A'_{66})], \qquad A_{\phi\phi} = \left[D'_{66} - \left(B'^2_{66}/A'_{66}\right)\right]\\
A_{m\kappa} &= \left[D'_{11} - \left(B'^2_{16}/A'_{66}\right)\right], \qquad A_{m\phi} = [D'_{16} - (B'_{16}B'_{66}/A'_{66})]\\
A_{\gamma\tau} &= 1/A'_{66}, \qquad A_{\phi\tau} = B'_{66}/A'_{66}, \qquad A_{n\tau} = A'_{16}/A'_{66}\\
A_{m\tau} &= B'_{16}/A'_{66}, \qquad A_{xn} = k\left[A_{55} - \left(A^2_{45}/A_{44}\right)\right]
\end{aligned} \tag{7a}$$

The factor k in A_{xn} is the Timoshenko shear correction factor accounting for the parabolic distribution of the shear stress across the thickness of the shell wall. In the present calculations, a value of $k = \frac{5}{6}$ has been used, although better estimates of this are available for specific lay-ups. Note that this factor takes into account the thickness effect of the shell wall. Additionally, there are global shear correction factors that depend on the blade cross section and that are derived later in the paper.

C. Derivation of the Cross Section Stiffness Relations

It is convenient to use a modified form of Reissner's[16] semicomplementary energy function Φ_R (Ref. 15)

$$\Phi_R = \left[N_{xx}\varepsilon_{xx} + M_{xx}\kappa_{xx} + M_{xs}\kappa_{xs} + N_{xn}\gamma_{xn}^k - N_{xs}\gamma_{xs}^k\right] \tag{8}$$

With this definition, we have

$$\begin{aligned}
\frac{\partial\Phi_R}{\partial\varepsilon_{xx}} &= N_{xx}, \qquad \frac{\partial\Phi_R}{\partial\kappa_{xx}} = M_{xx}, \qquad \frac{\partial\Phi_R}{\partial\kappa_{xs}} = M_{xs}\\
\frac{\partial\Phi_R}{\partial\gamma_{xn}^k} &= N_{xn}, \qquad \frac{\partial\Phi_R}{\partial N_{xs}} = -\gamma_{xs}^k
\end{aligned} \tag{9}$$

To obtain the stiffness matrix relating beam forces to beam displacements we use

$$\delta\int_0^l\int_C \left(\Phi_R + \gamma_{xs}^c N_{xs}\right)\mathrm{d}s\,\mathrm{d}x = 0 \tag{10}$$

where l is the length of the blade.

Using the equilibrium equations of the shell wall, we can get the shear flow as[17]

$$N_{xs} = N_{xs}^{(1)} + N_{xs}^{(2)} = \lfloor f\rfloor\lfloor\bar{q}_b\rfloor^T + \lfloor g_y g_z g_\omega\rfloor\lfloor V_y V_z T_\omega\rfloor^T \tag{11}$$

In Eq. (12),

$$\lfloor f\rfloor = \lfloor f_x f_z f_y f_\omega f_\phi\rfloor, \qquad \lfloor\bar{q}_b\rfloor = \lfloor U_{,x}\beta_{y,x}\beta_{z,x}\phi_{,xx}\phi_{,x}\rfloor \tag{12}$$

and the section shear flow variables $f_i (i = x, y, z, \omega, \phi)$ are determined as

$$f_x = \frac{\oint A_{n\tau}\,\mathrm{d}s}{\oint A_{\gamma\tau}\,\mathrm{d}s}, \qquad f_y = \frac{\oint A_{n\tau}y\,\mathrm{d}s + \oint A_{m\tau}z_{,s}\,\mathrm{d}s}{\oint A_{\gamma\tau}\,\mathrm{d}s}$$

$$f_z = \frac{\oint A_{n\tau}z\,\mathrm{d}s - \oint A_{m\tau}y_{,s}\,\mathrm{d}s}{\oint A_{\gamma\tau}\,\mathrm{d}s}$$

$$f_\omega = \frac{-\oint A_{n\tau}\bar{\omega}\,\mathrm{d}s + \oint A_{m\tau}q\,\mathrm{d}s}{\oint A_{\gamma\tau}\,\mathrm{d}s}, \qquad f_\phi = \frac{2A_0 - 2\oint A_{\phi\tau}\,\mathrm{d}s}{\oint A_{\gamma\tau}\,\mathrm{d}s} \tag{12a}$$

The subscript j denotes jth cell of the section. For open-cross-section beams, Eq. (13) becomes

$$f_i = 0 \qquad \text{for} \qquad i = (x, y, z, \omega, \phi) \tag{13}$$

Equation (11) gives a closed-form equation for the shear flow in terms of the assumed strains, their derivatives, and the cross-sectional properties of the blade. $N_{xs}^{(1)}$ is that part of the shear flow due to St. Venant torsion and the elastic couplings. In Eq. (11), g_y, g_z, and g_ω are functions that depend on the cross-sectional geometry and material properties and are required to calculate the shear coefficients for the first-order shear deformation theory. The expressions for $N_{xs}^{(2)}$ are analogous to those derived by Gjelsevik[20] for isotropic, uncoupled beams.

Using the value of N_{xs} from Eqs. (11) in Eq. (10), we can identify the cross-sectional stress resultants as

$$N = \int_C N_{xx}\,\mathrm{d}s, \qquad T_s = \int_C \left[-N_{xs}^{(1)}(r - \bar{\omega}_{,s}) - 2M_{xs}\right]\mathrm{d}s$$

$$M_y = \int_C [N_{xx}z - M_{xx}y_{,s}]\,\mathrm{d}s, \qquad Q_y = \int_C [N_{xs}y_{,s} + N_{xn}z_{,s}]\,\mathrm{d}s$$

$$M_z = \int_C [N_{xx}y + M_{xx}z_{,s}]\,\mathrm{d}s, \qquad Q_z = \int_C [N_{xs}z_{,s} - N_{xn}y_{,s}]\,\mathrm{d}s$$

$$M_\omega = \int_C [-N_{xx}\bar{\omega} + M_{xx}q]\,\mathrm{d}s \tag{14}$$

Using the relation for the torque, $T = T_s + T_\omega$ in Eq. (15), we obtain the stiffness relation for the beam as

$$\bar{\boldsymbol{F}} = \bar{\boldsymbol{K}}\bar{\boldsymbol{q}} \tag{15}$$

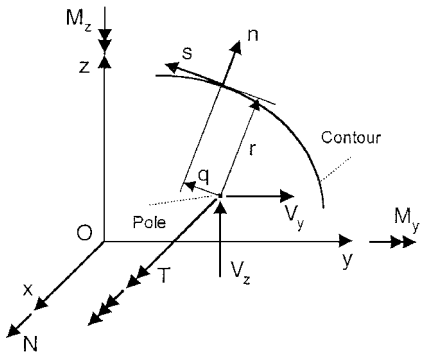

Fig. 2 Generalized beam forces and moments.

where

$$\bar{\boldsymbol{q}}^T = [U_{,x} \quad \gamma_{xy} \quad \gamma_{xz} \quad \phi_{,x} \quad \beta_{y,x} \quad \beta_{z,x} \quad \phi_{,xx}] \tag{15a}$$

$$\bar{\boldsymbol{F}}^T = [N \quad Q_y \quad Q_z \quad T_s \quad M_y \quad M_z \quad M_\omega] \tag{15b}$$

Figure 2 shows the generalized beam forces acting on the blade. The (7×7) stiffness matrix $\bar{\boldsymbol{K}}$ in Eq. (16) represents the beam stiffness matrix at a Timoshenko level of approximation.

D. Finite Element Equations of Motion

The governing differential equations of motion for a rotating composite beam can be derived by using Hamilton's principle:

$$\int_{t_1}^{t_2} (\delta\Pi_s - \delta T)\,\mathrm{d}t = 0 \tag{16}$$

where t_1 and t_2 are arbitrary instants of time and $\delta\Pi_s$ and δT are the variation of potential energy and the variation of kinetic energy, respectively. The variation of potential energy can be written by using the beam force-displacement relations, Eq. (15), as

$$\begin{aligned}\delta\Pi_s = \int_0^l \Big\{ & N\delta U_{,x} + M_z\delta\beta_{z,x} + M_y\delta\beta_{y,x} + M_\omega\delta\phi_{,xx} + T\delta\phi_{,x} \\ & + Q_y(\delta\beta_z + \delta V_{,x}) + Q_z(\delta\beta_y + \delta W_{,x}) + \underline{F_0 V_{,x}\delta V_{,x}} \\ & + \underline{F_0 W_{,x}\delta W_{,x}} + \underline{F_0 k_A^2 \phi_{,x}\delta\phi_{,x}} \Big\}\mathrm{d}x \end{aligned} \tag{17}$$

where F_0 is the centrifugal force defined at a spanwise beam coordinate x as

$$F_0 = \int_x^l m\Omega^2 x\,\mathrm{d}x \tag{17a}$$

The last three terms underscored in Eq. (17) are from the centrifugal stiffening terms due to rotation of the blade. Note that the higher-order nonlinear terms have been neglected in describing the strain energy expression, except for the centrifugal stiffening terms, because the latter play a significant role in the structural dynamics.[21] The variation of kinetic energy for a rotating composite beam can be written as

$$\delta T = \int_0^l \int_A \rho \boldsymbol{V}\cdot\delta\boldsymbol{V}\,\mathrm{d}A\,\mathrm{d}x \tag{18}$$

where ρ is the mass density, A is the area of the cross section, and $\boldsymbol{V}$ is the velocity vector for a given point on the deformed beam. Following the procedures described in Refs. 21 and 22, we get

$$\begin{aligned}\delta T = \int_0^l m\Big\{ & (\Omega^2 x + 2\Omega\dot{V} - \ddot{U})\delta u + (\Omega^2 V - 2\Omega\dot{U} - \ddot{V})\delta V \\ & - \ddot{W}\delta W - \Big[k_m^2\ddot{\phi} + \underline{\Omega^2\big(k_{m_2}^2 - k_{m_1}^2\big)\phi}\Big]\delta\phi \\ & + \underline{k_{m_2}^2\ddot{\beta}_z\delta\beta_z + k_{m_1}^2\ddot{\beta}_y\delta\beta_y}\Big\}\mathrm{d}x \end{aligned} \tag{19}$$

The term appearing in Eq. (19) underscored by one line is associated with tennis racket effect and those underscored by two lines are associated with rotary inertia effects of the section. The inertia effects associated with torsion warping are considered small and, thus, neglected in this study. Similar equations were formulated by Song and Librescu[23] for a thin-walled beam taking into account the effects of elastic couplings, transverse shear, and primary and secondary (thickness) warpings. This model was used to study the free vibration behavior of rotating composite beams. The effects of inertial warpings as well as centrifugal and Coriolis terms were incorporated, but only the membrane action of shell wall was retained in their analysis.

Three different types of interpolation functions are used to describe the behavior of the beam. For the axial displacement U, a four-node Lagrangian representation is used. The cross-sectional rotations (β_y and β_z) and the transverse deformations (V and W) are interpolated using a three-node Lagrangian shape function. For twist deformation ϕ and its derivative $\phi_{,x}$, a two-node Hermite shape function is employed to satisfy the C^1 continuity at each extremity of an element. These yield a total of 20 degrees of freedom for each finite element. The final set of equations of motion for the free vibration behavior of composite beams in terms of nodal degrees of freedom $\boldsymbol{q}_d$ can be written as

$$\boldsymbol{M}\ddot{\boldsymbol{q}}_d + \boldsymbol{C}\dot{\boldsymbol{q}}_d + \boldsymbol{K}\boldsymbol{q}_d = 0 \tag{20}$$

where $\boldsymbol{M}$, $\boldsymbol{C}$, and $\boldsymbol{K}$ are the finite element system of inertia, damping, and stiffness matrices, respectively. For simplicity, the effects of Coriolis terms are neglected by assuming that the beam axis is perpendicular to the axis of rotation.[24]

III. Results and Discussion

The present method has been used to analyze the vibration characteristics of rotating and nonrotating composite beams with various cross-sectional shapes and material distributions. The examples considered in this study include composite beams of box section, rectangular solid section, and I section. A numerical study was carried out to examine the convergence behavior of the current beam finite element model and to determine the number of finite elements required to obtain a desired accuracy of the solution. The present results are obtained using 12 spanwise beam finite elements.

A. Rotating Box Beam

Results for composite cantilevered box beams with bending–torsion or extension–torsion couplings and rotating at a constant speed Ω are presented first. For bending–torsion coupled beams, the ply layups in the opposite walls of the box section are symmetric (mirror image) with respect to beam axis, whereas for extension–torsion coupled beams, the corresponding layups are antisymmetric. The material properties and physical dimensions of the box beams considered are presented in Table 1.

Tables 2 and 3 show the comparison of natural frequencies for rotating box beams with symmetric and antisymmetric layups, respectively. The symmetric beam has ply layups of $[15]_6$ for top and bottom walls and $[15/-15]_3$ for side walls, whereas the antisymmetric beam has ply layups of $[15]_6$ for each wall of the box section. Note that the elastic coupling results in coupled mode shapes. For convenience, the modes that are predominantly bending and predominantly torsion are referred to as bending and torsion modes,

Table 1 Material properties and dimensions of graphite-epoxy box beams

Property	Dimensions
E_{11}	141.9 GPa (20.59×10^6 psi)
E_{22}	9.78 GPa (1.42×10^6 psi)
G_{12}	6.13 GPa (0.89×10^6 psi)
ν_{12}	0.42
ρ	1449 kg/m^3 (0.05224 lb/in.^{3})
Ply thickness t_p	0.127 mm (0.005 in.)
Outer width $2b$	24.21 mm (0.953 in.)
Outer depth $2h$	13.64 mm (0.537 in.)
Length l	844.6 mm (33.25 in.)

Table 2 Rotating natural frequencies (hertz) of a bending–torsion coupled box beam ($[15]_6$, $[15/-15]_3$ at $\Omega = 1002$ rpm)

Mode	Chandra and Chopra[26] Experiment	Chandra and Chopra[26] Analysis	Stemple and Lee[25]	Smith and Chopra[5]	Present mixed: Without shear	Present mixed: With shear
Flap 1	35.2	35.4	36.00	36.87	35.64	35.58
Lag 1	53.8	56.0	57.10	62.45	56.66	56.39
Flap 2	188.0	194.0	197.3	203.0	196.2	193.8
Lag 2	N/A	N/A	349.3	378.9	354.3	343.4
Torsion 1	N/A	N/A	714.9	729.2	702.2	701.7

Table 3 Rotating natural frequencies (hertz) of an extension-torsion coupled box beam ($[15]_6$ at $\Omega = 1002$ rpm)

Mode	Chandra and Chopra[26] Experiment	Chandra and Chopra[26] Analysis	Stemple and Lee[25]	Smith and Chopra[5]	Present mixed: Without shear	Present mixed: With shear
Flap 1	33.6	34.0	34.63	36.49	33.99	33.87
Lag 1	46.6	45.9	47.31	53.73	45.68	45.45
Flap 2	184.0	185.0	188.0	202.2	184.8	182.1
Lag 2	N/A	N/A	287.2	328.2	285.3	277.5
Torsion 1	N/A	N/A	513.2	493.7	495.5	495.5

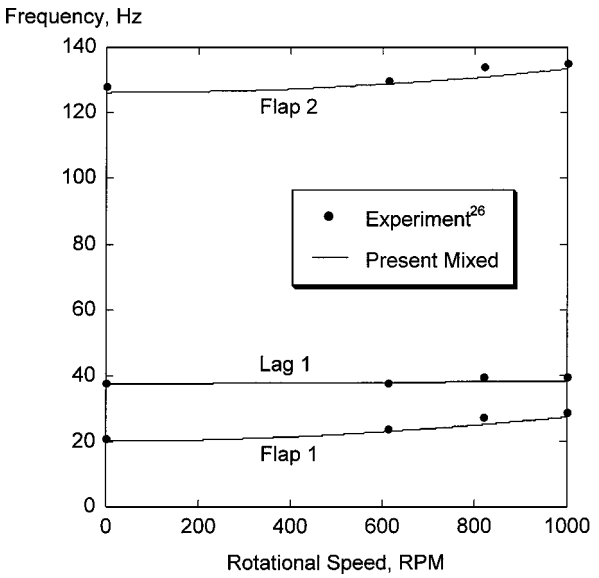

Fig. 3 Comparison of natural frequencies of $[30]_6$ bending–torsion coupled box beams at various rotational speeds.

respectively. Five normal modes (two flap, two lag, and one torsion) are examined. In Tables 2 and 3, the finite element analysis results of Stemple and Lee[25] and Smith and Chopra[5] are presented along with the experimental and theoretical results of Chandra and Chopra.[26] Reference 25 used a shear flexible beam element to model the warping of the cross section using a finite element discretization. Reference 5 used a shear-flexible beam model with refined description of constitutive relations to capture the two-dimensional in-plane elasticity behavior. The present results are obtained by using the mixed approach with and without transverse shear flexibility. The results show that the present predictions of mixed formulation with transverse shear show a good correlation with experimental data for both symmetric (Table 2) and antisymmetric (Table 3) configurations. The maximum error between the two sets of results is within 4%.

Figure 3 shows the influence of rotational speed on the calculated and experimental values of the first three fundamental frequencies (two flap and one lag) for a $[30]_6$ symmetric layup graphite-epoxy box beam. The data were taken from Ref. 26. Good correlation between these two results is obtained.

Table 4 Material properties of graphite-epoxy beams with rectangular solid section

Property	Dimensions
E_{11}	129.1 GPa (18.73×10^6 psi)
E_{22}	9.408 GPa (1.364×10^6 psi)
G_{23}	2.541 GPa (0.3686×10^6 psi)
G_{13}	4.304 GPa (0.6242×10^6 psi)
G_{12}	5.157 GPa (0.7479×10^6 psi)
ν_{12}	0.3
ρ	1551 kg/m^3 (0.056 lb/in.^{3})

B. Nonrotating Rectangular Solid Beams

Abarcar and Cunniff[27] presented the results of experimental and theoretical analysis on the vibration of cantilevered composite beams of rectangular cross section. Graphite-epoxy beams with fiber orientation of 15 and 30 deg tested in Ref. 27 are considered in the present study. The dimensions of the beam are length 190 mm, width 12.7 mm, and thickness 3.175 mm. The material properties used in the calculation are given in Table 4.

Tables 5 and 6 show the correlation of the free vibration results obtained by the present mixed method with experimental data and also with those obtained by other analyses: theoretical results from Abarcar and Cunniff[27] based on a flexibility approach, numerical results from Suresh and Nagaraj[28] using a stiffness approach and a torsional warping function based on a minimal strain energy, numerical results from Hodges et al.[29] based on a finite element approach, and numerical results from Stemple and Lee[25] based on a detailed finite element modeling. In Ref. 29, the cross-sectional stiffnesses were obtained from nonhomogeneous anisotropic beam section analysis (NABSA), and a finite element method was used to obtain the dynamic characteristics. In Tables 5 and 6, the first eight normal modes including lag bending (LB) modes (which were not investigated in Ref. 27) are presented. The flap-torsion (FT) and torsion-flap (TF) modes denote predominantly flap and predominantly torsion modes, respectively. In Tables 5 and 6, the present predictions consist of two parts that are designated as present 1 and 2, respectively. The second approach uses a more accurate description of the torsion related warping,[28,30] details of which are described in the Appendix. It is seen from Tables 5 and 6 that by applying enhanced warping models, the present predictions of bending modes along with torsion modes show good correlation with experimental data. The correlation is generally within 5% of measured values.

C. Rotating Rectangular Solid Beams

The present analysis has been used to obtain the frequencies of rotating composite solid beams tested by Epps and Chandra.[31] Graphite-epoxy beams of fiber angles 0 and 30 deg with zero tip sweep angle are considered. The numerical results obtained by Hodges et al.[9] are also presented for comparison. Hodges et al.[9] developed a geometrically nonlinear beam formulation for the analysis of initially curved and twisted composite beams. A two-dimensional finite element discretization for the cross section is necessary for the section coefficients, and VABS[2] is used for this purpose. The length of the beam is 952.5 mm and width 25.4 mm. The thickness of the beam is 2.97 mm and 3.12 mm for the 0- and 30-deg beams, respectively. Figures 4 and 5 show the comparison of rotating natural frequencies obtained by using the present analysis with the experimental data for 0-deg (Fig. 4) and 30-deg (Fig. 5) beams, respectively. The present predictions are in a good agreement with those of Hodges et al.[9] and with experimental data.[31] The correlation is generally within 5% for flap modes and 10% for the torsion mode. The increase in the flap mode frequencies due to rotation is significant, even for higher modes. This is correctly predicted for both beams.

D. Rotating I Beam

The rotating composite I beams tested by Chandra and Chopra[32] are used for validation. The material properties and dimensions of the beams are given in Table 7. Figure 6 shows the layup details of the symmetric I beams. The beam is composed of $[(0/90)_2/(90/0)/\theta_2]_T$

Table 5 Natural frequencies (hertz) of a 15-deg bending–torsion coupled composite beam with rectangular solid section

Mode no.	Abarcar and Cunniff[27] Experiment	Abarcar and Cunniff[27] Analysis	Suresh and Nagaraj[28]	Hodges et al.[29]	Stemple and Lee[25]	Present 1 (basic warping)	Present 2 (enhanced warping)
1 (FT)	82.5	80.8	82.2	77.4	85.0	82.2	82.2
2 (LB)	N/A	N/A	N/A	307.3	336.2	329.2	329.2
3 (FT)	511.3	501.5	511.4	479.2	527.4	511.8	511.7
4 (FT)	1423.4	1376.0	1411.1	1317.3	1469.3	1415.4	1411.6
5 (TF)	1526.9	1579.3	1588.6	1476.0	1543.1	1742.9	1578.5
6 (LB)	N/A	N/A	N/A	1836.5	2000.5	2062.9	2062.9
7 (FT)	2783.6	2648.7	2742.3	N/A	2903.7	2747.6	2744.9
8 (FT)	4364.6	4189.0	4368.4	N/A	4496.0	4413.7	4367.5
9 (TF)	4731.6	4772.5	4834.2	4517.2	N/A	5290.3	4826.7

Table 6 Natural frequencies (hertz) of a 30-deg bending-torsion coupled composite beam with rectangular solid section

Mode no.	Abarcar and Cunniff[27] Experiment	Abarcar and Cunniff[27] Analysis	Suresh and Nagaraj[28]	Hodges et al.[29]	Stemple and Lee[25]	Present 1 (basic warping)	Present 2 (enhanced warping)
1 (FT)	52.7	52.7	52.6	49.0	53.8	52.7	52.7
2 (LB)	N/A	N/A	N/A	195.6	214.1	210.7	210.7
3 (FT)	331.8	329.3	329.1	307.9	335.9	329.2	329.2
4 (FT)	924.7	915.9	918.0	869.1	941.1	918.6	918.6
5 (LB)	N/A	N/A	N/A	1215.2	1315.7	1320.4	1320.4
6 (FT)	1766.9	1767.0	1777.3	N/A	1707.0	1786.9	1762.9
7 (TF)	1827.4	1896.5	1891.6	1660.9	1881.1	2052.1	1836.6
8 (FT)	2984.0	2901.4	2929.9	N/A	3154.1	2946.0	2944.6

Table 7 Material properties and dimensions of Kevlar-epoxy I beams

Property	Dimensions
E_{11}	75.8 GPa (11×10^6 psi)
E_{22}	5.51 GPa (0.8×10^6 psi)
G_{23}	2.07 GPa (0.3×10^6 psi)
G_{13}	2.07 GPa (0.3×10^6 psi)
G_{12}	2.34 GPa (0.34×10^6 psi)
ν_{12}	0.34
ρ	1241 kg/m^3 (0.04482 lb/in.^{3})
Ply thickness t_p	0.2286 mm (0.009 in.)
Width $2b$	25.4 mm (1 in.)
Height $2h$	12.7 mm (0.5 in.)
Length l	844.55 mm (33.25 in.)

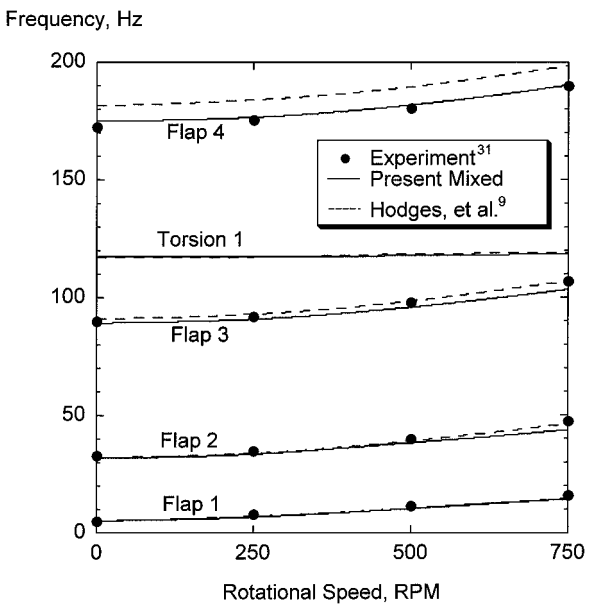

Fig. 4 Comparison of rotating natural frequencies of $[0]_{24}$ graphite-epoxy rectangular solid cantilevered beams.

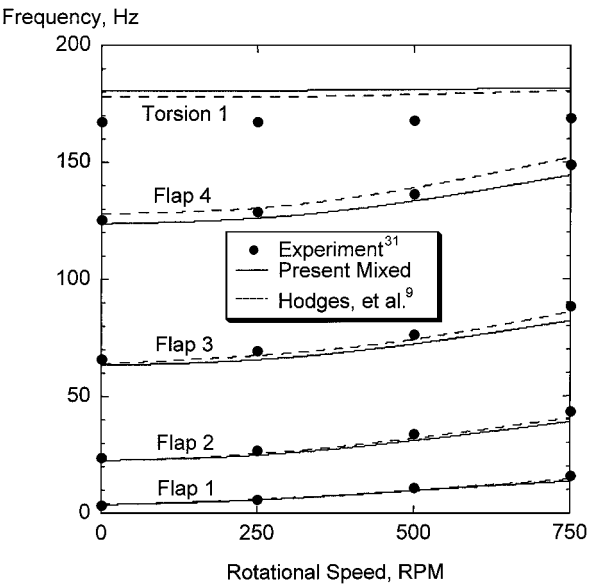

Fig. 5 Comparison of rotating natural frequencies of $[30]_{24}$ graphite-epoxy rectangular solid cantilevered beams with bending–torsion couplings.

for top and bottom flanges and $[0/90]_{2s}$ for web. Figure 7 shows the influence of rotational speed on the fundamental flap, lag, and torsion modes of a Kevlar®-epoxy 45-deg I beam. The correlation for the first flap mode obtained by using the current analysis is within 15% of test values. The influence of warping restraint effects on the open-section I beam is also presented. The warping restraint effect is seen to be significant for the torsion mode, but is negligible for bending modes.

An assessment has been made to improve this correlation. Because the I section is composed of two flanges and one web, and each part of the I-section can be regarded as a rectangular solid section, the expressions for flap, torsion, and coupling stiffnesses of the I-section beam can be modified as

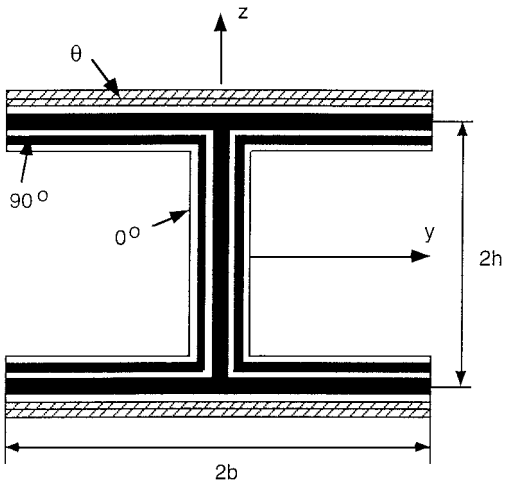

Fig. 6 Layup configuration of a bending–torsion coupled I beam.

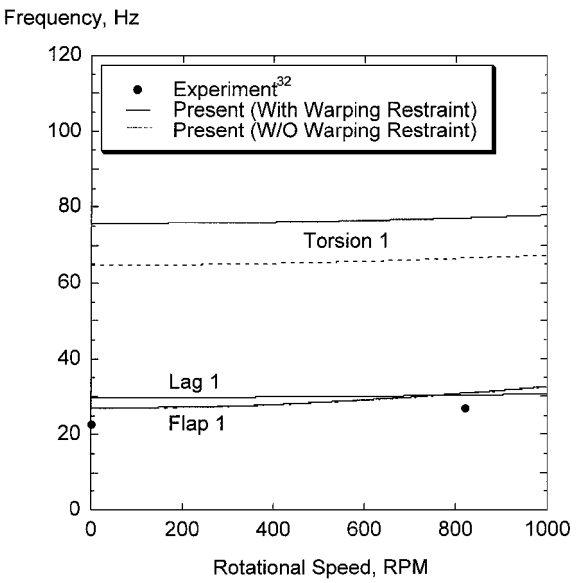

Fig. 7 Influence of rotational speed on natural frequencies of Kevlar-epoxy 45-deg I beam with bending-torsion couplings.

$$(\bar{K}_{55})_r = 2\left[\bar{K}^f_{55} - \lambda^f_0 \cdot \left(\bar{K}^f_{45}\right)^2 / \bar{K}^f_{44}\right] + \left[\bar{K}^w_{55} - \lambda^w_0 \cdot \left(\bar{K}^w_{45}\right)^2 / \bar{K}^w_{44}\right]$$

$$(\bar{K}_{45})_r = 2\bar{K}^f_{45} \cdot \left(1 - \lambda^f_0\right) + \bar{K}^w_{45} \cdot \left(1 - \lambda^w_0\right)$$

$$(\bar{K}_{44})_r = 2\bar{K}^f_{44} \cdot \left(1 - \lambda^f_0\right) + \bar{K}^w_{44} \cdot \left(1 - \lambda^w_0\right) \qquad (21)$$

where λ^f_0 and λ^w_0 are warping parameters for the flanges and web of the I section, respectively. Figure 8 shows the correlation with experiments for the rotating composite I beams. A slightly better correlation is obtained owing to the introduction of the enhanced warping model.

E. Influence of Thickness

Figure 9 presents the influence of wall thickness on the fundamental frequency of rotating symmetric layup (bending–torsion coupled) graphite-epoxy box beams. The physical properties of the box beam used in the calculation are given in Table 1. The beams are rotating at 1002 rpm. The layup for top and bottom flanges of the box beam is $[15]_{2n}$ and that for side flanges is $[15/-15]_n$. The parameter n is varied from 1 to 26. When n is equal to 26, the total number of layers in the box-beam wall is 52, and the thickness-to-depth ratio of the section is 0.48. The thickness-to-depth ratio is defined as the ratio of the wall thickness t divided by the outer depth $2h$ of the section. It is seen in Fig. 10 that wall thickness effects become larger as the wall thickness increases. Neglecting

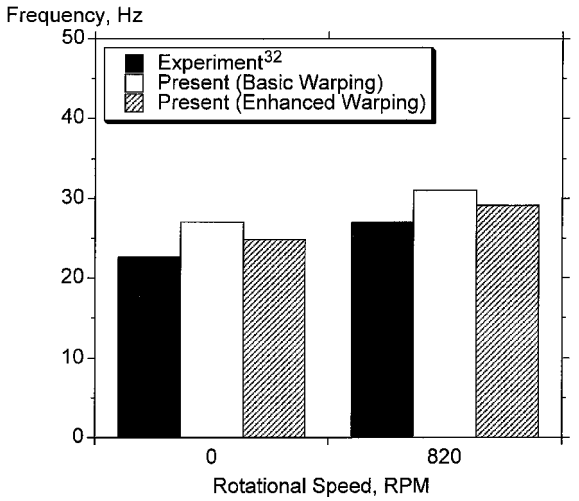

Fig. 8 Effects of enhanced warping on the fundamental flap mode of Kevlar-epoxy 45-deg I beam with bending-torsion couplings.

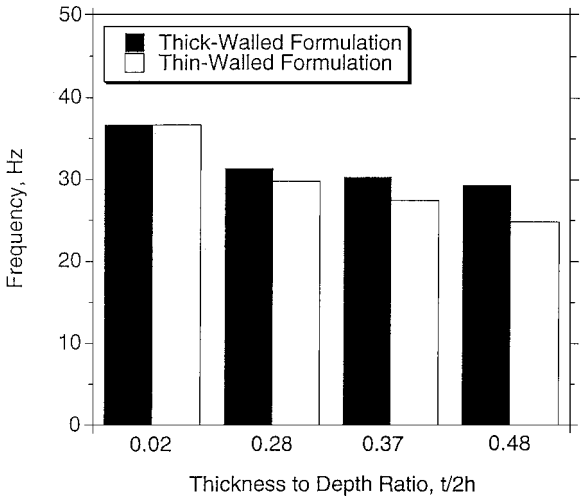

Fig. 9 Effects of wall thickness on the fundamental flap mode of 15-deg composite cantilevered box beams with bending-torsion couplings ($\Omega = 1002$ rpm).

wall thickness effects implies that the shell wall does not have any bending stiffness, and this assumption can result in an error in the prediction of frequency values of the beam. The error exceeds 10% for thickness-to-depthratios above 0.3. Note that the flap mode frequency becomes smaller as the wall thickness increases. Because the outer dimension of the box section is held fixed, the distance between the midplanes of the box-beam walls are getting closer with the increase in wall thickness. This results in lower section inertia that can cancel out the amount of increase in stiffness induced by a larger thickness. Because the mass of the beam grows steadily with the increase of thickness, the frequency values become smaller as the wall thickness increases. The effects of wall thickness on the flap mode frequencies of the bending–torsion coupled beam are presented in Fig. 10 for a thickness-to-depthratio of 0.28. The wall thickness effects are seen to be greater for higher modes. The difference between the thin- and the thick-walled formulation is 8% for the third mode, whereas the difference is 4% for the first flap mode.

Figure 11 shows the influence of wall thickness on the fundamental flap mode frequency for a rotating extension–torsion coupled composite box beam. For this calculation, each of the four box-beam walls has layup of $[15]_{2n}$, which yields extension–torsion couplings. The physical dimension and material properties of the beam are same as those of the bending–torsion coupled beam. To show the wall thickness effects, the thickness of the beam is again increased while both the outer dimension of the box section and the length of the beam are held fixed. Figure 11 shows that the influence

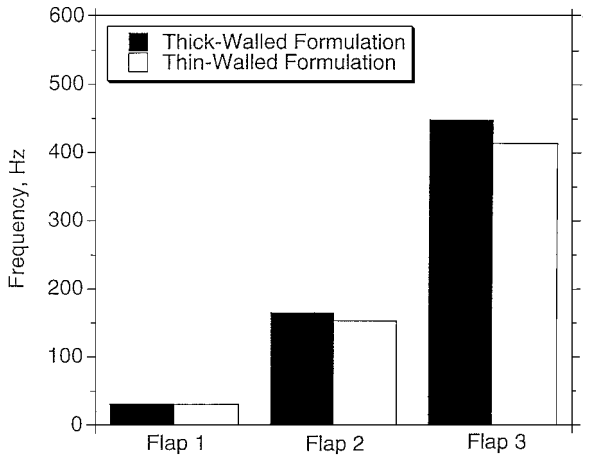

Fig. 10 Effects of wall thickness on flap mode frequencies of bending–torsion coupled composite box beams at a thickness to depth ratio of 0.28 (Ω = 1002 rpm).

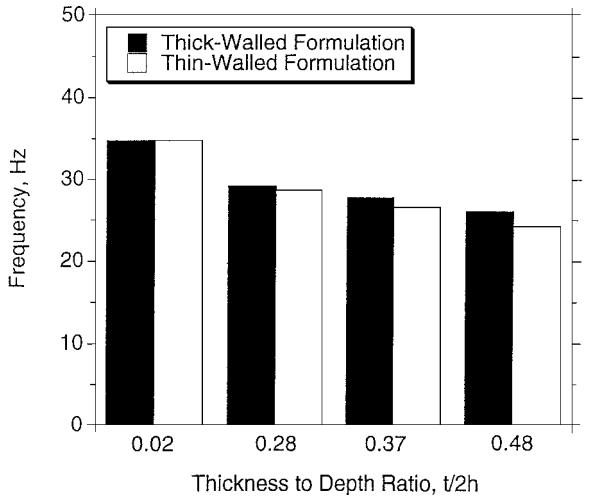

Fig. 11 Effects of wall thickness on the fundamental flap mode of 15-deg composite cantilevered box beams with extension–torsion couplings (Ω = 1002 rpm).

of wall thickness becomes larger for beams with higher thickness-to-depth ratios. However, the change in frequency values with increasing thickness-to-depth ratio is seen to be smaller than that of bending–torsion coupled beams (Fig. 9). At a thickness-to-depth ratio of 0.48, the percentage difference is 7.1% for the extension–torsion coupled beam (Fig. 11), whereas for the bending–torsion coupled beam (Fig. 9), the difference is 15.3%.

F. Effect of Transverse Shear

The effects of transverse shear deformation on the structural response of rotating composite box beams were investigated. In Fig. 12, the percentage error in the first flap mode frequency due to the neglect of transverse shear for both the extension–torsion coupled box beam ($[15]_6$) and the bending–torsion coupled box beam ($[15]_6$ for top and bottom flanges and $[15/-15]_3$ for side flanges) is plotted as a function of the slenderness ratio of the beam. The slenderness ratio is defined as the ratio of length to depth of a beam. The details of the box beam are provided in Table 1. The rotational speed of the beam is 1002 rpm. The percentage error in Fig. 12 is defined as $|\omega_s - \omega_{ns}|/\omega_s \times 100$, where ω_s and ω_{ns} are rotating flap frequencies obtained with and without transverse-shear couplings, respectively. As can be seen in Fig. 12, the slenderness ratio has a significant influence on the free vibration behavior of the beam. For the extension–torsion coupled beams with up to a slenderness ratio of 20, the percentage error between the two predictions is less than 5%, whereas for beams with a slenderness ratio of 5, the error becomes about 50%. Figure 12 shows that the influence of transverse shear is

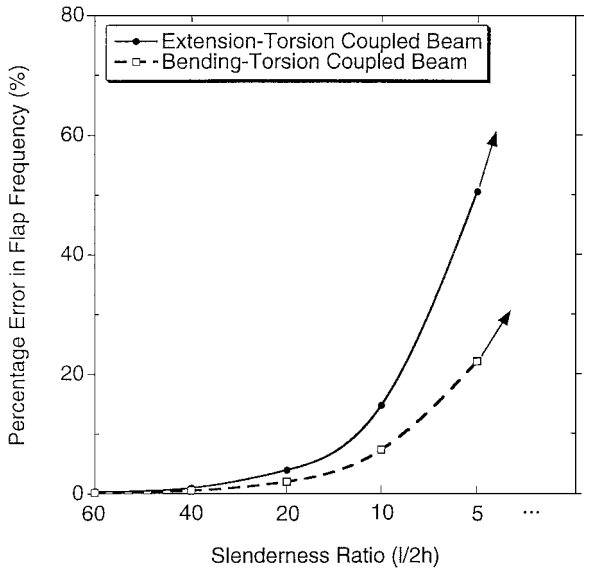

Fig. 12 Percentage error in flap mode frequencies due to the neglect of transverse shear for both the extension-torsion and bending-torsion coupled composite box beams (Ω = 1002 rpm).

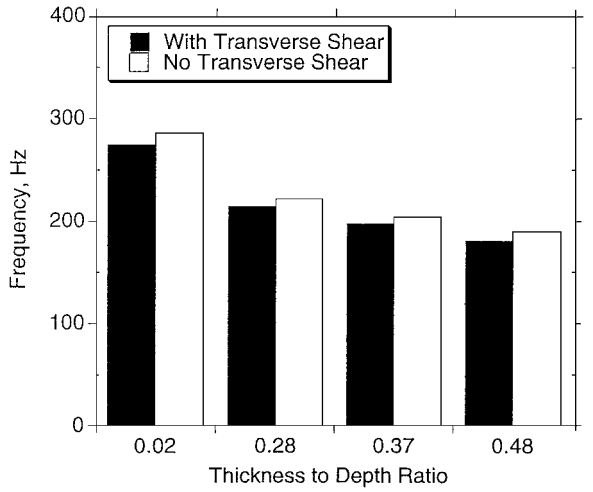

Fig. 13 Effects of transverse shear as a function of thickness to depth ratio on flap mode frequency of extension–torsion coupled composite box beams at a slenderness ratio of 20 (Ω = 1002 rpm).

more for the extension–torsion coupled beams than for the bending–torsion coupled beams. One reason for this is that the elastic couplings are introduced only through the top and bottom flanges for bending–torsion coupled beams, whereas for the extension–torsion coupled beams the couplings are introduced through all four walls of the box section. Hence, the shear couplings of bending–torsion coupled beams play a lesser role than those of extension–torsion coupled beams. The other reason is that, for the bending–torsion coupled beams, the transverse shear couplings affect not only the bending modes, but also the torsion modes, because the shear strains γ_{xz} and γ_{xy} are kinematically coupled with transverse displacements [see Eq. (2a)]. These shear strains influence the torsional stiffness via bending–torsion couplings. However, for the extension–torsion coupled beam, the torsional stiffness is not affected by transverse shear couplings because the shear strains influence only the bending stiffnesses via bending–shear couplings. Because the shear strains influence both bending and torsional stiffnesses for the bending–torsion coupled configuration beams, the transverse shear effects on the flap mode frequency become smaller than those for extension–torsion coupled beams.

Figure 13 shows the influence of transverse shear on the flap mode frequency with varying thickness-to-depth ratios of composite box beams. For the calculation, each of the four walls of the box

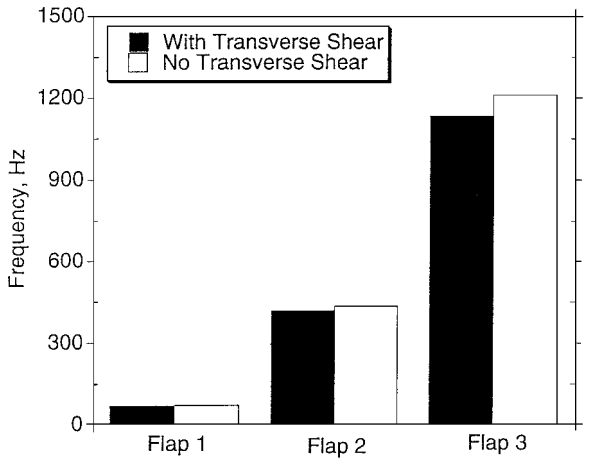

Fig. 14 Effects of transverse shear on flap mode frequencies of extension–torsion coupled composite box beams at a slenderness ratio of 40 ($\Omega = 1002$ rpm).

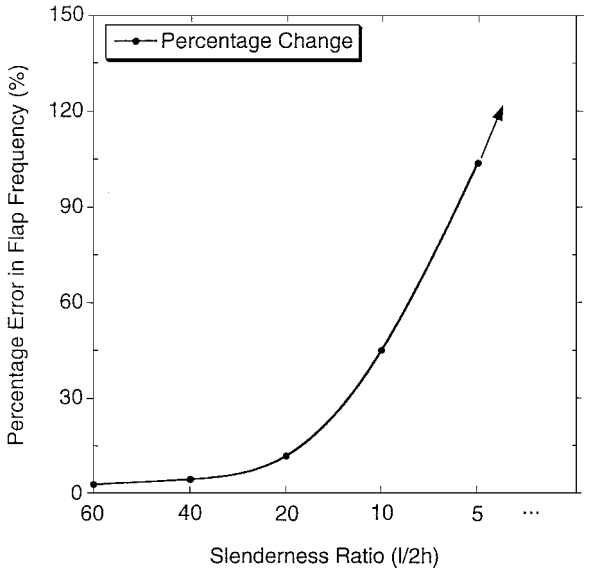

Fig. 15 Percentage error in flap mode frequency due to the neglect of transverse shear for the extension–torsion coupled composite I beam ($\Omega = 1000$ rpm).

section has a layup of $[15]_{2n}$, and n is varied from 1 to 26. This beam configuration displays extension–torsion and bending–shear couplings. A reduction in the flap frequency by the introduction of transverse–shear couplings is obtained for beams with different thickness-to-depthratios. Figure 14 represents the effects of transverse shear on rotating natural frequencies of a $[15]_6$ extension–torsion coupled composite box beam. The slenderness ratio of the beam is set to 40. It is seen that the transverse shear reduces the flap frequencies by around 7% for the third flap mode compared with 1% for the first mode. This reduction in the frequency values is due to the additional flexibility in the flap bending stiffness provided through the transverse–shear couplings. Note that the change in the flap frequency is greater for higher modes.

Figure 15 shows the effects of transverse shear on the flap frequency as a function of slenderness ratio for an extension–torsion coupled composite I beam. The layup of the I section is $[(0/90)_2/(90/0)/15_2]_T$ for flanges and $[0/90]_{2s}$ for web, respectively. The slenderness ratio of the beam has a large influence on the vibration behavior of the open-section I beam. As slenderness ratio decreases, the transverse shear effects become more significant, and the deviation between the predictions with and without transverse shear couplings become larger. The error due to the neglect of transverse shear is 3% for a slendernessratio of 60, but the error increases to over 100% for a slenderness ratio of 5.

IV. Conclusions

A refined structural dynamics model applicable to both thick- and thin-walled composite beams that can have open- or closed-profile sections has been formulated. The theory accounts for the effect of elastic coupling, shell-wall thickness, warping, warping restraint, and transverse shear deformation. The free vibration analysis has been correlated against experimental data and other analyses for rotating and nonrotating composite beams of various cross sections. The beams include box-section, rectangular solid section, and I-section beams. Correlation of natural frequencies for the coupled beams was good for box beams and satisfactory for rectangular solid section and I-section beams. An assessment was made to improve the correlation of the open-section beams, and, by using a refined cross-sectional warping, a better correlation was obtained. The wall thickness effects are shown to be significant in predicting vibration frequencies, especially for bending–torsion coupled beams. For such beams, the wall thickness effects become significant when the thickness-to-depthratio of the beam reaches around 30%. At this ratio, the error in frequency due to neglecting of wall thickness ratio becomes 10%. The effects are larger for the higher modes.

Transverse–shear flexibility shows significant effects on the vibration modes of elastically coupled composite box and I beams. The transverse–shear couplings are shown to have a larger influence on the extension–torsion coupled beams than on the bending–torsion coupled beams. The effect becomes larger for beams with high slendernessratios. For an extension–torsion coupled box beam with a slenderness ratio of 5, the frequency error due to the neglect of transverse shear is about 50%, whereas the error is within 1% for a box beam with slenderness ratios of greater than 40. It is shown also that the influence of transverse–shear couplings is greater for higher modes.

Appendix: Influence of Thickness on Torsional Stiffness

For beams with rectangular solid sections, the higher-order warping effects are known to be significant in accurately predicting the behavior of a beam.[28,30] Use of the equations of equilibrium relating M_{xs} and N_{xn} leads to a better approximation to the curvature κ_{xs}, which in turn leads to a warping correction λ_0 that is defined as

$$\lambda_0 = 0.6274 \cdot \tanh\left(\frac{\pi}{2} \cdot \frac{b}{h} \cdot \sqrt{\frac{G_{xz}}{G_{xy}}}\right) \Big/ \left(\frac{b}{h} \cdot \sqrt{\frac{G_{xz}}{G_{xy}}}\right) \qquad \text{(A1)}$$

where G_{xz}/G_{xy} is the ratio of shear moduli referred to as the beam axes. This constant λ_0 will be used in the section stiffness coefficients to account for the effects of the higher-order warping (thickness warping). For uncoupledorthotropicbeams of rectangular solid section, the correction is the same as that proposed by Ritchie and Rosinger.[30] The ratio of shear moduli shown in Eq. (A1) can be expanded for beams of general anisotropic layups and is expressed as the ratio of in-plane compliance coefficients:

$$\sqrt{G_{xz}/G_{xy}} = \sqrt{S_{66}/S_{55}} \qquad \text{(A2)}$$

where

$$S_{55} = A_{44}\big/\left(A_{44}A_{55} - A_{45}^2\right), \qquad S_{66} = \left(A_{11}A_{22} - A_{12}^2\right)\big/|A_{ij}|$$

A_{ij} represent in-plane stiffness coefficients for a given laminate[19] and $|A_{ij}|$ denotes the determinant of the matrix A_{ij}. For bending–torsion coupled beams of rectangular solid section, the stiffness values given in Eq. (19) are modified as

$$(\bar{K}_{55})_r = 2b\left(A_{m\kappa} - \lambda_0 A_{m\phi}^2/A_{\phi\phi}\right), \qquad (\bar{K}_{45})_r = -4bA_{m\phi}(1-\lambda_0)$$

$$(\bar{K}_{44})_r = 8bA_{\phi\phi}(1-\lambda_0) \qquad \text{(A3)}$$

As one can see from Eq. (A3), the magnitude of stiffness coefficients becomes reduced due to the warping correction. As the thickness-to-depthratio of a section increases, the thickness warpings become larger, and this results in a reduction in the stiffness values. Neglecting this effect leads to a poorer correlation with experimental data, especially in a material whose principal shear moduli differ appreciably.

Acknowledgments

This work was supported by the National Rotorcraft Technology Center under Grant NCC 2944. Technical Monitor was Yung Yu. The first author was also supported partially by the Korea Science and Engineering Foundation under the postdoctoral fellowship program.

References

[1]Jung, S. N., Nagaraj, V. T., and Chopra, I., "Assessment of Composite Rotor Blade Modeling Techniques," *Journal of the American Helicopter Society*, Vol. 44, No. 3, 1999, pp. 188–205.

[2]Cesnik, C. E. S., and Hodges, D. H., "VABS: A New Concept for Composite Rotor Blade Cross-Sectional Modeling," *Journal of the American Helicopter Society*, Vol. 42, No. 1, 1997, pp. 27–38.

[3]Rehfield, L. W., "Design Analysis Methodology for Composite Rotor Blades," Seventh DOD/NASA Conf. on Fibrous Composites in Structural Design, AFWAL-TR-85-3094, Denver, CO, June 1985, pp. (v̈(a)1–v̈(a)15).

[4]Rehfield, L. W., Atilgan, A. R., and Hodges, D. H., "Nonclassical Behavior of Thin-Walled Composite Beams with Closed Cross Sections," *Journal of the American Helicopter Society*, Vol. 35, No. 2, 1990, pp. 42–51.

[5]Smith, E. C., and Chopra, I., "Formulation and Evaluation of an Analytical Model for Composite Box-Beams," *Journal of the American Helicopter Society*, Vol. 36, No. 3, 1991, pp. 23–35.

[6]Chandra, R., and Chopra, I., "Experimental and Theoretical Analysis of Composite I-Beams with Elastic Couplings," *AIAA Journal*, Vol. 29, No. 12, 1991, pp. 2197–2206.

[7]Chandra, R., and Chopra, I., "Structural Behavior of Two-Cell Composite Rotor Blades with Elastic Couplings," *AIAA Journal*, Vol. 30, No. 12, 1992, pp. 2914–2921.

[8]Hodges, D. H., Atilgan, A. R., Cesnik, C. E. S., and Fulton, M. V., "On a Simplified Strain Energy Function for Geometrically Nonlinear Behavior of Anisotropic Beams," *Composites Engineering*, Vol. 2, Nos. 5–7, 1992, pp. 513–526.

[9]Hodges, D. H., Shang, X., and Cesnik, C. E. S., "Finite Element Solution of Nonlinear Intrinsic Equations for Curved Composite Beams," *Journal of the American Helicopter Society*, Vol. 41, No. 4, 1996, pp. 313–321.

[10]Mansfield, E. H., and Sobey, A. J., "The Fiber Composite Helicopter Blade, Part I: Stiffness Properties, Part II: Prospects for Aeroelastic Tailoring," *Aeronautical Quarterly*, Vol. 30, Pt. 2, May 1979, pp. 413–449.

[11]Libove, C., "Stress and Rate of Twist in Single-Cell Thin-Walled Beams with Anisotropic Walls," *AIAA Journal*, Vol. 26, No. 9, 1988, pp. 1107–1118.

[12]Johnson, E. R., Vasiliev, V. V., and Vasiliev, D. V., "Anisotropic Thin-Walled Beams with Closed Cross-Sectional Contours," *Proceedings of the AIAA/ASME/ASCE/AHS/ASC 39th Structures, Structural Dynamics, and Materials Conference*, AIAA, Reston, VA, 1998, pp. 500–508.

[13]Berdichevsky, V. L., Armanios, E., and Badir, A., "Theory of Anisotropic Thin-Walled Closed-Cross-Section Beams," *Composites Engineering*, Vol. 2, Nos. 5–7, 1992, pp. 411–432.

[14]Badir, A. M., Berdichevsky, V. L., and Armanios, E. A., "Theory of Composite Thin-Walled Opened-Cross-Section Beams" *Proceedings of the AIAA/ASME/ASCE/AHS/ASC 34th Structures, Structural Dynamics, and Materials Conference*, AIAA, Washington, DC, 1993, pp. 2761–2770.

[15]Murakami, H., Reissner, E., and Yamakawa, J., "Anisotropic Beam Theories with Shear Deformation," *Journal of Applied Mechanics*, Vol. 63, No. 3, 1996, pp. 660–668.

[16]Reissner, E., "On a Certain Mixed Variational Theorem and a Proposed Application," *International Journal for Numerical Methods in Engineering*, Vol. 20, No. 7, 1984, pp. 1366–1368.

[17]Jung, S. N., Nagaraj, V. T., and Chopra, I., "A General Structural Model for Thin- and Thick-Walled Composite Blades with Elastic Couplings," 24th European Rotorcraft Forum, Marseilles, France, Sept. 1999.

[18]Palazotto, A. N., and Dennis, S. T., *Nonlinear Analysis of Shell Structures*, AIAA, Washington, DC, 1992, p. 33.

[19]Jones, R. M., *Mechanics of Composite Materials*, McGraw–Hill, New York, 1975, Chap. 4.

[20]Gjelsvik, A., *The Theory of Thin Walled Bars*, Wiley, New York, 1981, pp. 19, 20, 105–109.

[21]Hodges, D. H., and Dowell, E. H., "Nonlinear Equations of Motion for the Elastic Bending and Torsion of Twisted Nonuniform Rotor Blades," NASA TN D-7818, 1974.

[22]Jung, S. N., and Kim, S. J., "Aeroelastic Response of Composite Rotor Blades Considering Transverse Shear and Structural Damping," *AIAA Journal*, Vol. 32, No. 4, 1994, pp. 820–829.

[23]Song, O., and Librescu, L., "Structural Modeling and Free Vibration Analysis of Rotating Composite Thin-Walled Beams," *Journal of the American Helicopter Society*, Vol. 42, No. 4, 1997, pp. 358–369.

[24]Kaza, K. R. V, and Kielb, R. E., "Effects of Warping and Pretwist on Torsional Vibration of Rotating Beams," *Journal of Applied Mechanics*, Vol. 51, No. 4, 1984, pp. 913–920.

[25]Stemple, A. D., and Lee, S. W., "Large Deflection Static and Dynamic Finite Element Analyses of Composite Beams with Arbitrary Cross-Sectional Warping," *Proceedings of the AIAA/ASME/ASCE/AHS/ASC 30th Structures, Structural Dynamics, and Materials Conference*, AIAA, Washington, DC, 1989, pp. 1788–1798.

[26]Chandra, R., and Chopra, I., "Experimental–Theoretical Investigation of the Vibration Characteristics of Rotating Composite Box Beams," *Journal of Aircraft*, Vol. 29, No. 4, 1992, pp. 657–664.

[27]Abarcar, R. B., and Cunniff, P. F., "The Vibration of Cantilever Beams of Fiber Reinforced Material," *Journal of Composite Materials*, Vol. 6, No. 10, 1972, pp. 504–517.

[28]Suresh, J. K., and Nagaraj, V. T., "Higher-Order Shear Deformation Theory for Thin-Walled Composite Beams," *Journal of Aircraft*, Vol. 33, No. 5, 1996, pp. 978–986.

[29]Hodges, D. H., Atilgan, A. R., Fulton, M. V., and Rehfield, L. W., "Free Vibration Analysis of Composite Beams," *Journal of the American Helicopter Society*, Vol. 36, No. 3, 1991, pp. 36–47.

[30]Ritchie, I. G., and Rosinger, H. E., "Torsional Rigidity of Rectangular Section Bars of Orthotropic Materials," *Journal of Composite Materials*, Vol. 9, April 1975, pp. 187–190.

[31]Epps, J. J., and Chandra, R., "The Natural Frequencies of Rotating Composite Beams with Tip Sweep," *Journal of the American Helicopter Society*, Vol. 41, No. 1, 1996, pp. 29–36.

[32]Chandra, R., and Chopra, I., "Analytical–Experimental Investigation of Free-Vibration Characteristics of Rotating Composite I Beams," *Journal of Aircraft*, Vol. 30, No. 6, 1993, pp. 927–934.

A. Berman
Associate Editor